Science of the Total Environment 905 (2023) 167294

Contents lists available at ScienceDirect

Science of the Total Environment

journal homepage: www.elsevier.com/locate/scitotenv

Comparative genomic analysis reveals electron transfer pathways of *Thermoanaerobacterium thermosaccharolyticum*: Insights into thermophilic electroactive bacteria

Xing Yan [a], Jie Bu [a], Xiong Chen [b], Ming-Jun Zhu [a,b,c,*]

[a] School of Biology and Biological Engineering, Guangdong Key Laboratory of Fermentation and Enzyme Engineering, South China University of Technology, Guangzhou Higher Education Mega Center, Panyu, Guangzhou 510006, People's Republic of China
[b] Key Laboratory of Fermentation Engineering (Ministry of Education), Hubei University of Technology, Wuhan 430068, Hubei, People's Republic of China
[c] The Key Laboratory of Biological Resources and Ecology of Pamirs Plateau in Xinjiang Uygur Autonomous Region, The Key Laboratory of Ecology and Biological Resources in Yarkand Oasis at Colleges & Universities under the Department of Education of Xinjiang Uygur Autonomous Region, College of Life and Geographic Sciences, Kashi University, Kashi, People's Republic of China

HIGHLIGHTS

- Extracellular Fe(III) and electrode respiration were firstly confirmed in *MJ2*.
- Detailed electrochemical and microscopic analysis methods were established.
- Comparative genomics elucidates the complete electron transfer pathway of *MJ2*.
- Inner membrane hydrogenase with cytochrome *c* mediates IET of *MJ2*.
- Cytochrome c bound to the outer membrane for EET of *MJ2* by forming a biofilm.

GRAPHICAL ABSTRACT

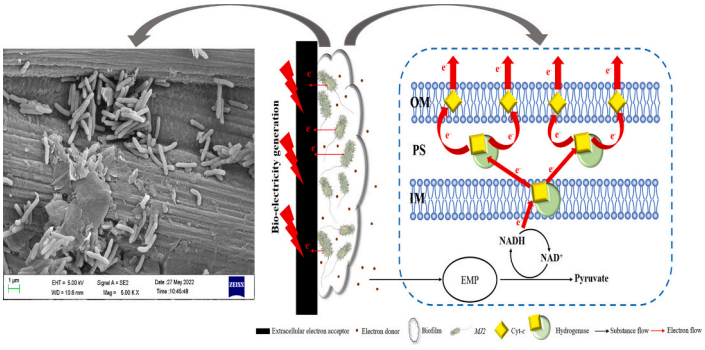

ARTICLE INFO

Editor: Huu Hao Ngo

Keywords:
Intracellular electron transfer
Extracellular electron transfer
Cytochrome c
Biofilms
Comparative genomic analysis

ABSTRACT

Microbial extracellular respiration is an important energy metabolism on earth, which is significant for the elemental biogeochemical cycle. Herein, extracellular Fe(III) and electrode respiration were confirmed in *Thermoanaerobacterium thermosaccharolyticum MJ2*. The intra/extracellular electron transfer (IET/EET) mechanism of *MJ2* was investigated by comparative genomic analysis for the first time. Morphological characterization and electrochemical properties of anode illustrated that *MJ2* generated bio-electricity by forming a biofilm. The respiration chain inhibition and enzyme activity tests showed that hydrogenase with cytochrome *c* (Cyt-*c*) was involved in IET of *MJ2*. Noteworthily, the exogenous Cyt-*c* increased hydrogenase activity to promote bio-electricity generation by 92.84 %. The Cyt-*c* gene synteny between *MJ2* and another well-known exoelectrogen (*Thermincola potens JR*) indicated that Cyt-*c* bound to the outer membrane mediated the formation of

* Corresponding author at: School of Biology and Biological Engineering, Guangdong Key Laboratory of Fermentation and Enzyme Engineering, South China University of Technology, Guangzhou Higher Education Mega Center, Panyu, Guangzhou 510006, People's Republic of China.
E-mail address: mjzhu@scut.edu.cn (M.-J. Zhu).

https://doi.org/10.1016/j.scitotenv.2023.167294
Received 4 January 2023; Received in revised form 27 August 2023; Accepted 21 September 2023
Available online 22 September 2023

biofilm involved in EET of *MJ2*. This study broadened the understanding of microbial extracellular respiration diversity and provided new insights to explore the electron transfer pathways of exoelectrogens.

1. Introduction

Microorganisms produce energy through a variety of metabolic modes, and extracellular respiration is a significant form of microbial energy metabolism (Hallbeck and Pedersen, 1990; Lovley and Phillips, 1988; Myers and Nealson, 1988). Microorganisms transfer electrons released from intracellular oxidation of organic matter to the extracellular matrix under anaerobic conditions, and the energy produced by the reduction of extracellular electron acceptors sustains their growth. Unlike conventional anaerobic respiration, the end terminal electron acceptor for extracellular respiration is extracellular. When electrons produced by extracellular respiration pass through the intracellular respiratory chain, it must pass across the non-conductive cell membrane/wall to electron acceptors that cannot enter the cell (Lovley et al., 2004; Weber et al., 2006). Some studies showed that insoluble metallic minerals, electrodes, humic substances could also be used as the electron acceptors for extracellular respiration by electroactive bacteria present in different environments (even extreme ones) (Koch and Harnisch, 2016; Logan et al., 2019; Lusk et al., 2015; Parameswaran et al., 2013). The discovery of microbial extracellular respiration is of great scientific significance and application value, which expands the understanding of the diversity of microbial energy metabolism and provides a scientific basis for the study of extracellular respiratory microorganisms and their respiratory modes. In addition, extracellular respiration has good application prospects in the fields of in in-situ remediation of pollutants, wastewater treatment, and lignocellulosic biomass energy recovery through enriched mixed culture of thermophilic bacteria in microbial fuel cell (MFC) technology (Anderson et al., 2003; Davila et al., 2011; Dopson et al., 2016; Lusk et al., 2018).

Currently, most studies have focused on extracellular electron transfer (EET) pathway in two model microbes (*Shewanella* and *Geobacter* species), including indirect electron transfer mediated through redox-active electron shuttles and direct electron transfer by conductive pili or cytochrome *c* (Cyt-*c*), such as Mtr, Cym, Omc and Ppc (Coursolle et al., 2010; Kondo et al., 2015). However, the intracellular electron transfer (IET) pathway of extracellular respiratory microorganisms remains unclear. In addition, the mining of extracellular respiratory microbial diversity is still limited. As mentioned earlier, the diversity of multihaem Cyt-*c* is directly related to the diversity of EET pathway, which is not only involved in the transfer of intracellular electrons from inner membrane (IM) to the periplasmic space (PS), but also has a large share in the outer membrane (OM) (Kugarajah and Dharmalingam, 2021). The resolution of the Cyt-*c* function that mediates direct electron transfer will contribute to the discovery of novel electron transfer pathway.

As well documented, comparative genomics is used to compare genomic features of a species or multiple species genomes based on genome mapping and sequencing technologies, such as structural and functional gene regions (Hols et al., 2005). By comparing the genome structure and identifying the similarities and differences with bioinformatics methods, it finds out the contraction and expansion of gene families between species, the differentiation time and evolutionary relationship, as well as the generation and evolution of new genes, etc., which has been widely used in clarifying the evolutionary relationship of species and revealing the function of genes (Li et al., 2019b). However, until now, no comparative genomic analysis has been reported to investigate the evolutionary relationships and functions of genes mediating EET in exoelectrogens.

In this work, the extracellular Fe(III) and electrode respiration ability of *Thermoanaerobacterium thermosaccharolyticum* MJ2 were carried out for the first time by chemical, electrochemical kinetics methods, and microscopic characterizations to understand its EET mainly through the biofilm. In addition, the electron transfer pathway was reconstructed by comparative genomic analysis, and its key site Cyt-c linking IET/EET was identified, and the biological function of Cyt-c was resolved, thus revealing its complete IET/EET mechanism and providing novel approaches for subsequent studies. This discovery is important for environmental and bioenergy applications of thermophilic bacteria, especially in capturing energy from the lignocellulosic biomass.

2. Materials and methods

2.1. Inoculum and culture condition

The thermophilic *MJ2* isolated from paper sludge (Donghua paper Co., Ltd., Guangdong, China) was cultured in the medium (1.3 g/L $(NH_4)_2{\cdot}SO_4$, 2.6 g/L $MgCl_2{\cdot}6H_2O$, 1.43 g/L KH_2PO_4, 5.5 g/L K_2HPO_4, 0.13 g/L $CaCl_2{\cdot}2H_2O$, 6 g/L Na_2-β-glycerophosphate$\cdot 5H_2O$, 1.1 mg/L $FeSO_4{\cdot}7H_2O$, 0.25 g/L Glutathione, 4.5 g/L Yeast extract, pH = 7.0) supplemented with 10 g/L xylan (Ryon biological technology Co., Ltd., Shanghai, China) for 16 h at 55 °C under anaerobic conditions (An et al., 2018).

2.2. Extracellular Fe(III) reduction tests

Extracellular Fe(III) reduction was performed in a serum bottle (total volume of 120 mL) containing 45 mL above medium supplemented with 10 g/L cellobiose as an electron donor. 0.5, 1, 2 and 4 g/L hematite (Fe_2O_3, 99.8 %, Aladdin, China) was supplied to the serum bottle as an electron acceptor. All medium were purged with N_2 for 30 min and sealed in serum bottles with rubber stoppers and aluminum lids, then kept at shaker (150 rpm) for 24 h at 55 °C (Gonzalez-Gil et al., 2005). 5 mL of the above cultures were inoculated to the serum bottles used as inoculum under sterile conditions.

2.3. Bio-electricity generation experiments

Microbial fuel cell (MFC) was composed of the anode/cathode chamber and proton exchange membrane (PEM, Nafion-117, Chemours). The effective volume for each chamber of MFC was 150 mL. The anode chamber contained 90 mL above medium supplemented with 10 g/L cellobiose as electron donor, while the cathode chamber was filled with 100 mL $K_3[Fe(CN)_6]$ (50 mM, dissolved in 50 mM phosphate buffer, pH = 7.0) as electron acceptor (Dai et al., 2017). PEM treated with H_2O_2 (5 %, w/w) at 80 °C for 1 h before use, followed by soaking in deionized water (Millipore, USA) for 30 min, then boiling in H_2SO_4 (5 %, w/w) at 80 °C for 1 h, and finally soaking in deionized water again for 30 min (Wu et al., 2018). Hydrophilic carbon paper (Taiwan carbon technology Co., Ltd.) was used as the electrode of MFC. The surface area of both the anode and cathode was 2.25 cm^2 (1.5 cm × 1.5 cm). The anode and cathode were connected by an external titanium wire and external resistor (2000 Ω). 10 mL of the above cultures were inoculated to the anode chamber was used as inoculum under sterile conditions. MFC was incubated in a shaker (150 rpm) at 55 °C for 24 h.

2.4. Morphological characterization

The morphological characterization of the anode was observed through FE-SEM (Carl Zeiss, Jena, Germany). The carbon paper anode was cut into small pieces (5 mm × 5 mm) and washed three times with 0.01 M phosphate buffer saline, fixed with 2.5 % (v/v) glutaraldehyde for 5 h, and then dehydrated with a series of alcohol solution (30, 50, 70,

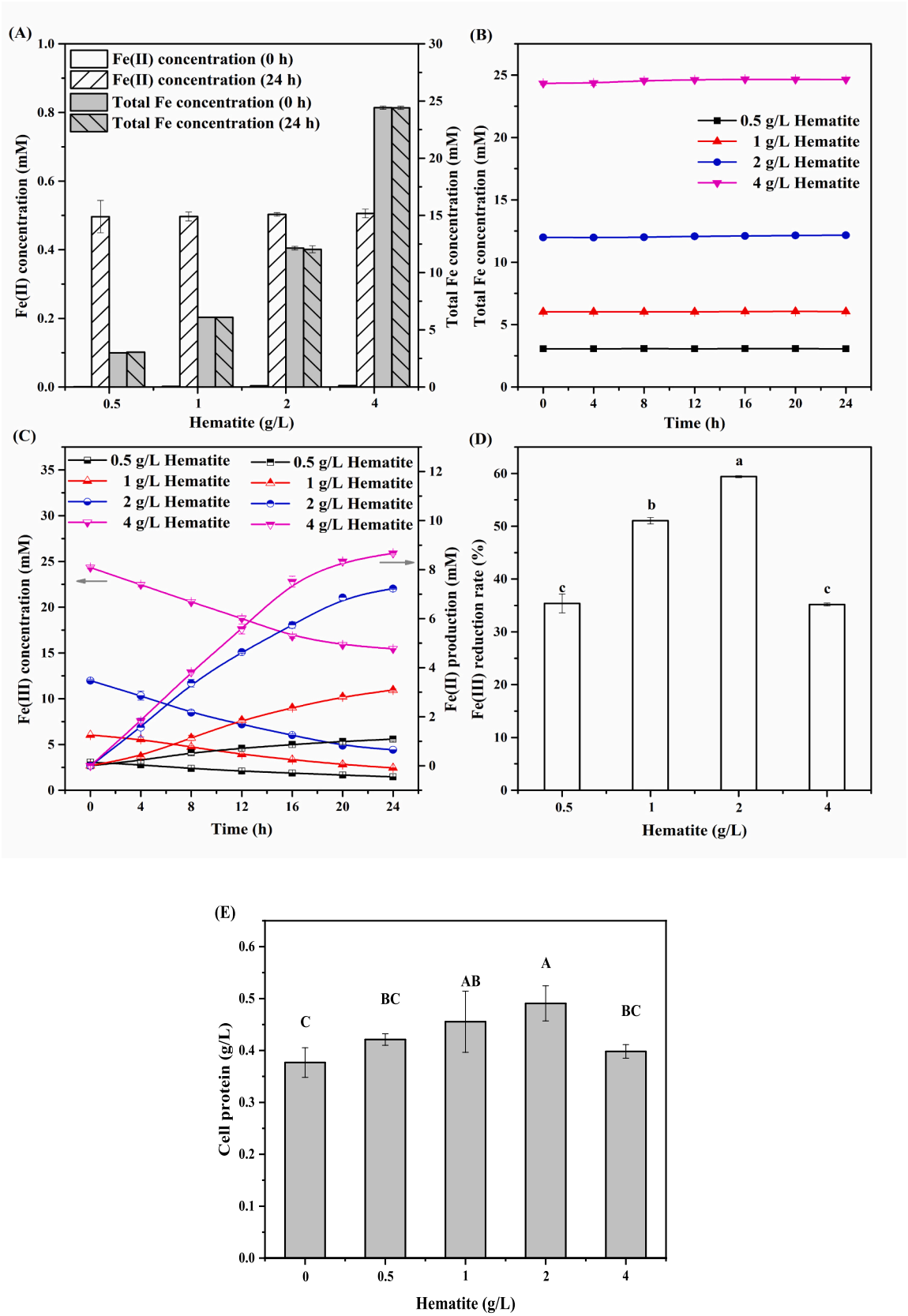

Fig. 1. Effect of hematite loadings on extracellular Fe(III) reduction of MJ2. (A) Abiotic control; (B) total Fe concentration; (C) Fe(III) concentration and Fe(II) production; (D) Fe(III) reduction rate; (E) Cell protein.

90, 95, 100 %, v/v). Finally, FE-SEM observation was performed after drying for 1 h with a critical evaporator (Tousimis, Autosamdri-815A, USA).

2.5. Electrochemical measurements

The cyclic voltammetry (CV) and differential pulse voltammetry (DPV) were performed to characterize the electrochemical properties of *MJ2* using an electrochemical workstation (CHI 650E, CH Instruments, Inc., Shanghai, China) under anaerobic conditions. All measurements were performed with suspensions of the anode chamber in the three-electrode system, in which the anode of MFC was set as the working electrode, the platinum plate as the counter electrode and the Ag/AgCl as the reference electrode. The CV test was carried out with the scan range of −2–1.6 V (vs. Ag/AgCl) and the scan rate of 20–200 mV/s (Bu et al., 2022). The DPV test conditions were as follows: scan range of potential, 0.55–1.25 V (vs. Ag/AgCl); amplitude, 50 mV; pulse width, 0.05 s; potential increment, 4 mV; quiet time, 2 s.

2.6. Electron transfer response assays

Before the bio-electricity generation process, five specific inhibitors (final concentration: 0.5 mM capsaicin, 0.5 mM rotenone, 0.5 mM dicumarol, 0.5 mM famoxadone and 20 mM tertiary butanol (TBA)) were added separately to the anode chamber as required to investigate the electron transfer pathway (Lian et al., 2016; Wang et al., 2021). Moreover, 10 μM flavins (98 %, Aladdin, China) and 1 μM Cyt-*c* (Meimian Industrial Co., Ltd., Jiangsu, China) were also added to the anode chamber to explore their effects on the electron transfer, respectively.

2.7. Complete genome-based comparative genomic analysis

The bioinformatics analysis (Fig. S1) includes complete genome sequencing and comparative genomic analysis. *MJ2* for complete genome sequencing was harvested by centrifugation (4 °C, 12,000 ×*g*, 5 min) 16 h after incubation, and was subsequently washed three times with normal saline. Genomic DNA was extracted with the SDS method. Libraries for SMRT sequencing was constructed with an insert size of 10 kb using the SMRT bell TM Template kit (Version 1.0). At last, the library quality was assessed on the Qubit® 2.0 Fluorometer (Thermo Fisher Scientific, USA) and detected the insert fragment size by Agilent 2100 (Agilent Technologies, USA). The complete genome of *MJ2* was sequenced using the PacBio Sequel platform at the Beijing Novogene Bioinformatics Technology Co., Ltd.

The comparative genomic analysis included genome visualization, phylogenetic analysis, pan-genome analysis, average nucleotide identity (ANI) and genomic synteny. The genome sequences and Cyt-*c* sequences of other typical exoelectrogens were obtained from NCBI database. A complete genome overview was created by CGView Server to visualize. The data was analyzed on the online platform of Majorbio Cloud Platform (www.majorbio.com). Genomic alignment between *MJ2* and reference genomes (*DX-1* and *JR*) was performed using NCBI-BLAST. Genomic synteny was analyzed by the TBtools program based on the alignment results (Chen et al., 2020).

2.8. Analytical methods

The Fe(II) and total Fe concentration were measured by the ferrozine colorimetric method with minor modification (Liu et al., 2019; Stookey, 1970). Briefly, 0.2 mL of samples, 0.8 mL of HCl (0.01 M) or $NH_2OH{\cdot}HCl$ (10 % w/v, dissolved in 0.01 M HCl) were mixed into a 2 mL centrifuge tube and placed in darkness for 1 h. After centrifuged at 12,000 ×*g* for 5 min, 0.1 mL of supernatants and 0.9 mL of ferrozine solution (0.1 % w/v, dissolved in 0.1 M CH_3COONH_4) were mixed to initiate the color reaction, measured at 562 nm. The Fe(III) reduction rate was calculated with Fe(II) compared with the concentration of total Fe.

The output voltage was recorded at 20 min intervals by a digital collector (Lilliput optoelectronics technology Co., Ltd., Fujian, China) connected to the external resistor. The output voltage curves were fitted with a modified Logistic equation:

$$U(t) = \frac{U_m}{1 + \frac{U_m - U_0}{U_0} \times e^{-a(1-bt)t}}$$

where the $U(t)$ is the output voltage, U_m is the peak voltage, U_0 is the initial voltage, a is the bio-electricity generation rate, b is the decay rate.

The flavins were measured by fluorescence spectrophotometer at an excitation wavelength of 450 nm and an emission wavelength of 520 nm (Lu et al., 2022). The Cyt-*c* was detected using a commercial enzyme-linked immunosorbent ELISA kit (Meimian Industrial Co., Ltd., Jiangsu, China). The cell protein and hydrogenase activity were analyzed as previously reported (Bu et al., 2021). To avoid the effect of cell protein concentration on hydrogenase activity, the units of hydrogenase activity were converted to mL-H_2/g-cell protein.

The electron transfer system activity (ETSA) was tested based on previous the 2-(*p*-iodophenyl)-3-(*p*-nitrophenyl)-5-phe-nyltetrazolium chloride (INT) method with minor modification (Huang et al., 2022). Briefly, 1 mL of samples, 3 mL of Tris-HCl (pH 8.6), and 2 mL of INT (0.2 %, w/v) were mixed into a 10 mL centrifuge tube and placed in a dark shaker (37 °C, 150 rpm) for 30 min. 2 mL of formaldehyde (37 %, v/v) was added to the centrifuge tube to terminate the reaction. Centrifuged the samples at 8000 ×*g* for 5 min and discarded the supernatant. 5 mL of methanol was then added to redissolve the precipitation. Finally, the samples were centrifuged at 5000 ×*g* for 5 min to measure the absorbance at 485 nm.

The results in this study were analyzed by one-way ANOVA and Duncan's multiple range test and presented as means ± standard deviation of three replicates of independent experiments. Statistical analysis was performed using the software SPSS (Version 17.0, Chicago, USA) to evaluate the significant difference ($P < 0.05$).

3. Results and discussion

3.1. Extracellular Fe(III) respiration of MJ2

In the absence of *MJ2*, the production of 0.5 mM Fe(II) was observed at different hematite loadings after 24 h of anaerobic incubation (Fig. 1A), indicating the presence of reducing substances in the medium. It might due to the presence of glutathione, which is an important antioxidant and free radical scavenger that binds to free radicals and heavy metals (Yang et al., 2022a). However, the content of glutathione was fixed in the medium, it did not change with hematite loadings. Obviously, this part of Fe(II) produced by abiotic action has been removed in the calculation of Fe(II) production and Fe(III) reduction rate. In addition, the differences in total Fe concentration between 0 h and 24 h were not significant ($P > 0.05$) with different hematite loadings in the presence and absence of *MJ2* (Fig. 1A–B), suggesting that the biosorption between hematite and *MJ2* and the abiotic interaction between hematite and the medium were negligible. This was contrary to the study of Jia et al. in which approximately 10 % decrease of insoluble minerals was observed, due to adsorption with microorganisms (Jia et al., 2021). This distinction might be caused by the difference in strains or culture conditions. Besides, the concentration of Fe(III) gradually decreased as the cultivation progresses in the presence of *MJ2*, while the production of Fe(II) increased up to 8.67 mM (Fig. 1C), indicating that the reduction of Fe(III) by microorganism was dominant. This phenomenon suggested that *MJ2* has Fe(III) reduction ability. It was able to transfer electrons generated from the metabolism of intracellular oxidized substrates to the extracellular insoluble hematite. A variety of *Shewanella* and *Geobacter* species in *Proteobacteria* had extracellular Fe (III) reduction ability (Koch and Harnisch, 2016; Logan et al., 2019; Lovley and Phillips, 1988; Myers and Nealson, 1988), and this was the

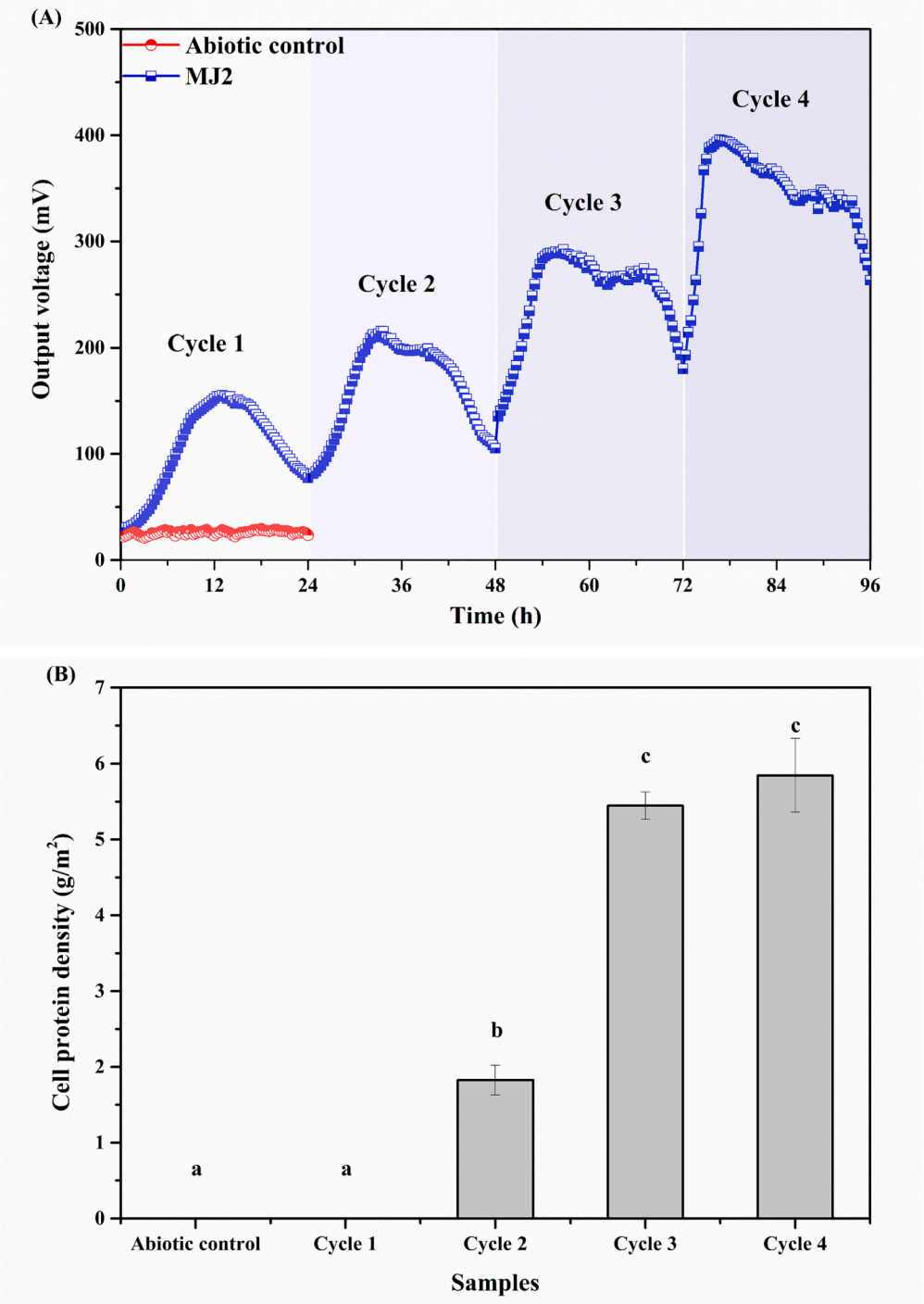

Fig. 2. Characterization of MFC of *MJ2*. (A) Bio-electricity generation performance; (B) Cell protein density of anode.

first report of *T. thermosaccharolyticum* in *Firmicutes*.

The kinetics fitting analysis (Fig. S2) indicated that the reduction of Fe(III) to Fe(II) followed the first-order kinetics with R^2 all above 0.97. The rate constant k increased and then decreased with the increase of hematite loadings up to 0.043 h^{-1} (2 g/L hematite). Additionally, the Fe (III) reduction rate reached the maximum (59.40 %) with hematite added at 2 g/L. However, the Fe(III) reduction rate decreased significantly ($P < 0.05$) with the increase of hematite to 4 g/L (Fig. 1D), indicating that the reduction of Fe(III) was significantly inhibited, probably due to the toxicity of high Fe(III) concentration on cells. To test the above conjecture, the cell protein concentration at different hematite loadings was measured, and the result was presented in Fig. 1E. As expected, the cell protein concentration also increased and then decreased with the hematite additions. The maximum cell protein concentration (0.49 g/L) was reached with 2 g/L hematite addition. When the addition of hematite was increased to 4 g/L, the cell protein was significantly lower ($P < 0.05$), indicating that *MJ2* was inhibited by Fe (III) at high concentrations of hematite additions. High-dosage magnetite nanoparticles can reduce the anaerobic digestion performance, and even ferrous ions caused ferroptosis of bacteria (Shen et al., 2020).

3.2. Extracellular electrode respiration of MJ2

The output voltage of *MJ2* MFC on the electrode under four

Table 1
The bio-electricity generation fitting of *MJ2* MFC in four cycles.

Cycle index	Peak voltage (mV)	Output voltage difference (mV)	R^2
1	153.63	131.53	0.98
2	207.83	139.05	0.95
3	280.36	168.70	0.91
4	363.22	187.18	0.74

consecutive cycles was tested, and the result was shown in Fig. 2A. Within each cycle, the output voltage increased first and then decreased with incubation time. While the output voltage of the abiotic control without the addition of *MJ2* did not change significantly, suggesting that the bio-electricity generation ability was correlated with inoculum (Koffi and Okabe, 2020). The output voltage curves during the four cycles were further fitted and the result was shown in Table 1. Both the peak voltage and output voltage difference were significantly increased with the index of cycles, suggesting that the electrogenic activity of *MJ2* increased, which may be the result of the gradual maturation of the *MJ2* MFC system. Many studies have reported that enriched electroactive colonies require a longer period of maturation to form biofilm structures and that *MJ2* of pure culture may also mediate bio-electricity generation through the establishment of biofilms (Huang et al., 2015; Michie et al., 2011; Yates et al., 2012). In addition, the output voltage difference increased by 21.32 % and 10.95 % from the second to the third cycle, and from the third to the fourth cycle, respectively, which is higher than the increase from the first to the second cycle (5.72 %), indicating that it may have formed the biofilm in the third or fourth cycle and thus reached a steady state.

To test the above hypothesis, FE-SEM observation (Fig. S3) was

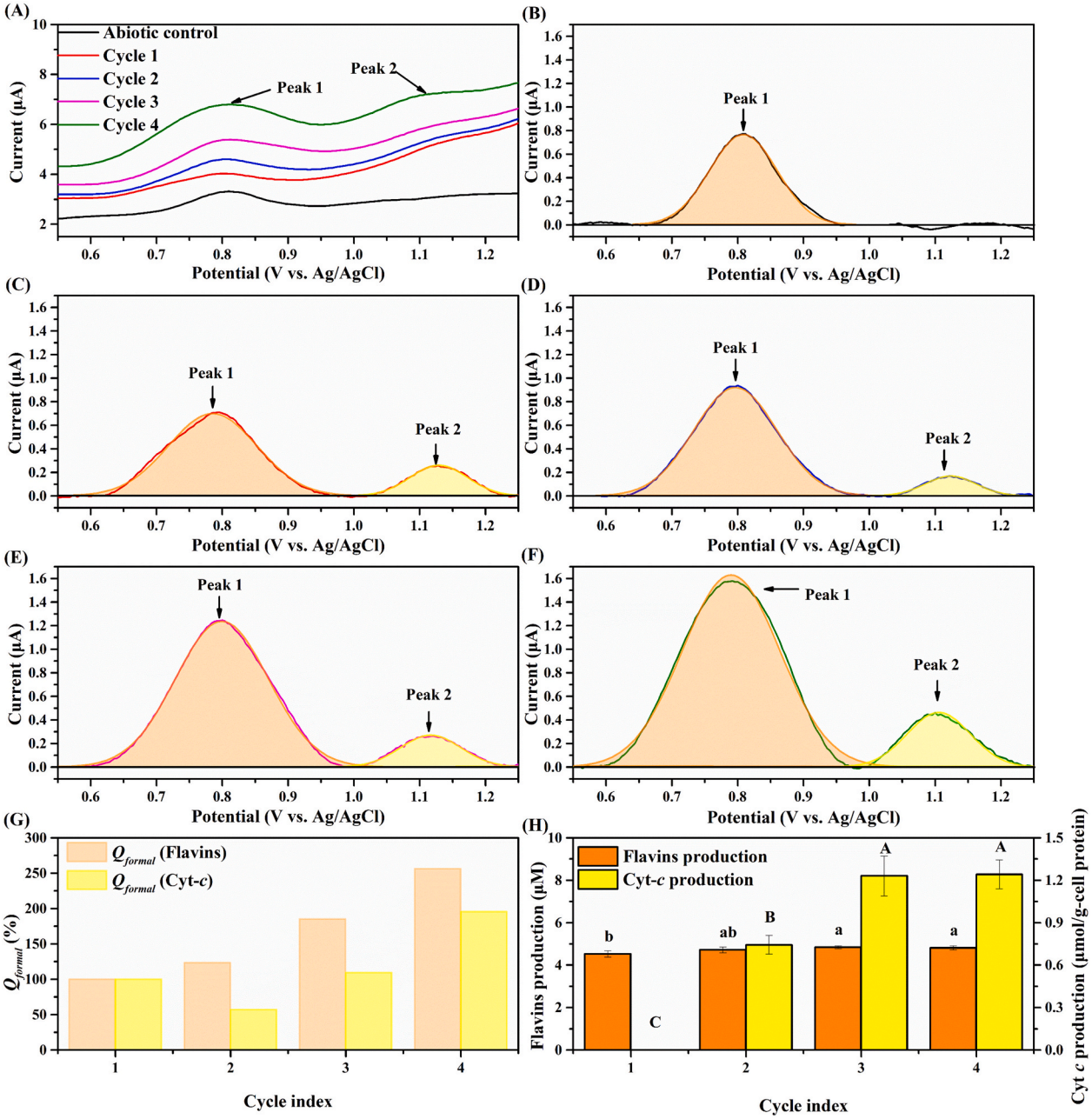

Fig. 3. The extracellular electrochemical properties of *MJ2*. (A) DPV scans; (B) Multi-peak resolution of abiotic control; (C) multi-peak resolution of cycle 1; (D) multi-peak resolution of Cycle 2; (E) multi-peak resolution of Cycle 3; (F) multi-peak resolution of Cycle 4; (G) comparison of redox activities of flavins/Cyt-*c* in different samples; (H) flavins and Cyt-*c* production.

Table 2
Genomic features of exoelectrogens.

Statistics	*MJ2*	*JR*	*DX-1*	*MR-1*	*PCA*	*PAO1*
Size (bp)	2,992,605	3,157,416	5,404,117	4,972,338	3,814,128	6,264,404
G + C%	33.73	45.88	65.44	45.96	60.94	66.56
Coding genes	3106	3001	4892	4192	3397	5572
rRNA	15	9	27	27	6	13
tRNA	57	52	49	105	48	63
sRNA	5	4	4	6	4	30
Genomic islands	17	9	9	17	11	6
Prophages	4	0	2	3	0	1

performed on four cycles of anode electrode, it can be seen that the anode surface of the abiotic control was smooth, with only some inorganic salt particles attached to the electrode. After the first cycle, no significant microbial attachment was observed on the anode surface, probably due to strains being loosely adsorbed to generate bio-electricity (Lee et al., 2004). At the end of the second cycle, some strains were observed to be attached to the surface of the carbon paper, and the bio-electricity generation was significantly increased during this period. In addition, at the end of the third and fourth cycles, the number of strains attached to the anode surface increased significantly. This

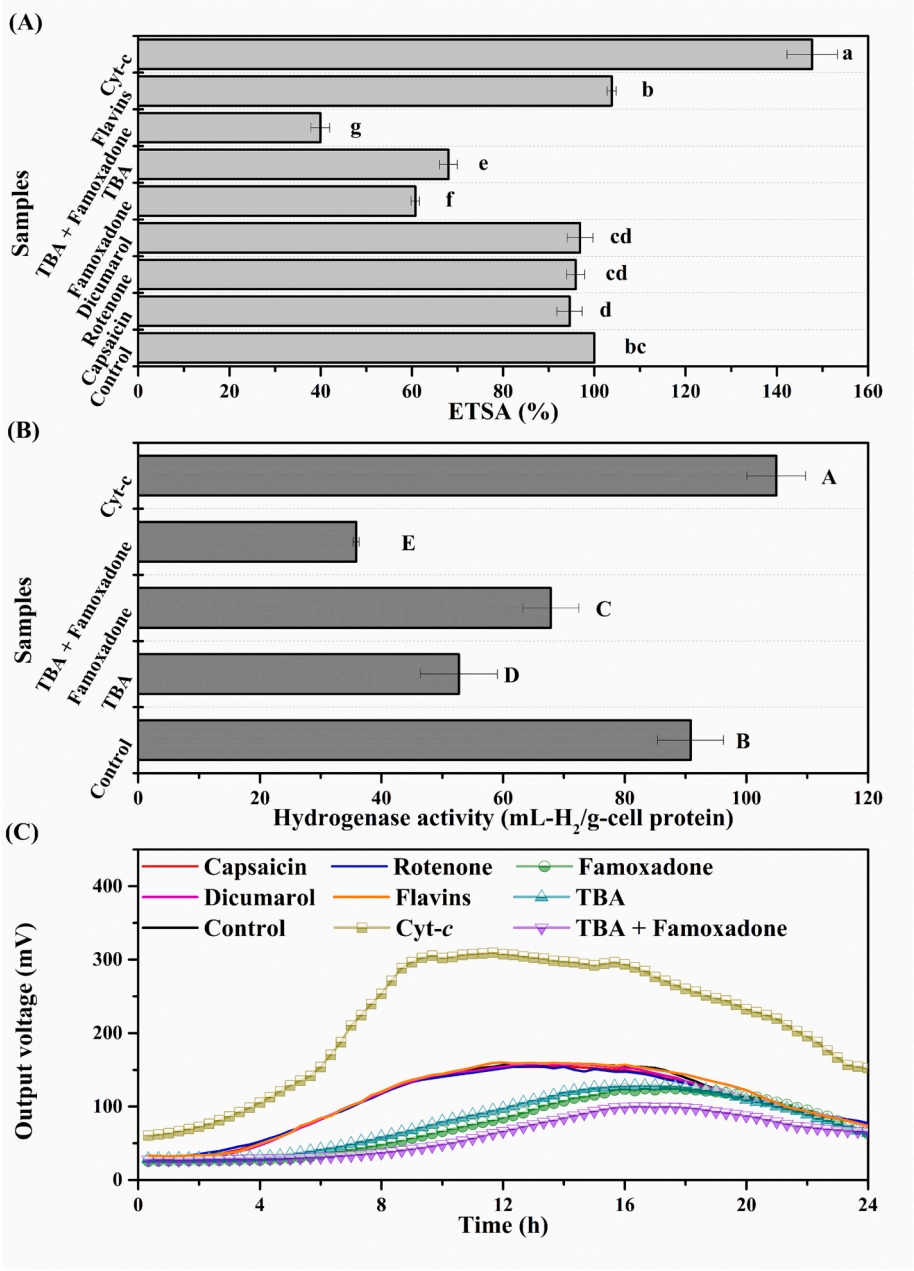

Fig. 4. Effect of flavins and Cyt-*c* on electron transfer of *MJ2*. (A) ETSA; (B) hydrogenase activity; (C) bio-electricity generation performance.

phenomenon was similar to the results for cell protein density of the anode (Fig. 2B). At the end of the first cycle, no cell protein was detected on the anode. The cell protein density of the anode was significantly higher in the second cycle than in the first cycle. And the further extension of the domestication time, the cell protein density of the anode continued to increase significantly ($P < 0.05$). However, the cell protein density of the anode in the fourth cycle did not increase significantly compared to the third cycle, indicating the formation of a stable biofilm structure (Hassan et al., 2018; Zhuang et al., 2020), which is the main way to mediate the bio-electricity generation of most Gram-negative electrogenic strains that bring the microorganisms into direct contact with the electrode (Saunders et al., 2020).

3.3. Extracellular electrochemical properties of MJ2

To further investigate the EET mechanism of *MJ2*, the extracellular electrochemical properties of the anode solution of *MJ2* MFC were performed by the CV (Fig. S4) and DPV scans. The presence of two anodic oxidation peaks was evident in the broad potential window spanned, which was attributed to the activity of flavins (Peak 1) and Cyt-*c* (Peak 2) electron transfer (Lu et al., 2022; Wang et al., 2018). In the abiotic control, only the flavins oxidation peak was observed, which may have been introduced from the yeast extract in the medium. Additionally, the peak currents increased linearly with the logarithm of the scan rates, suggesting that these redox reactions were typical electrochemical kinetic processes (Yin et al., 2018). Notably, no oxidation peak of Cyt-*c* was observed, further suggesting that Cyt-*c* was associated with the presence of *MJ2*. It has been reported that Cyt-*c* was mainly distributed on the OM of Gram-negative electrogenic strains and showed EET through direct contact between the OM and the extracellular electron acceptors (Li et al., 2019a). High sensitively DPV scans showed the characteristic peaks in the range of 0.55–1.25 V, attributed to flavins (0.79 V vs. Ag/AgCl) and Cyt-*c* (1.12 V vs. Ag/AgCl), respectively, whose function was mainly to mediate the EET of exoelectrogens (Fig. 3A). The current of the peaks (i_p) of both flavins and Cyt-*c* were increased with the index of cycles, also suggesting enhanced electroactivity of *MJ2*, which was consistent with the results of bio-electricity generation (Bu et al., 2022). A multi-peak fitting of the DPV curves showed a gradual increase in the peak areas of flavins and Cyt-*c*. As shown in Fig. 3B–F, the i_p of flavins increased from 4.03 μA to 6.78 μA, while the i_p of Cyt-*c* increased from 5.18 μA to 7.24 μA. Furthermore, by calculating the fitted peak areas (Fig. 3G), the relative Q_{formal} increased from 100 % to 256.30 % for flavins and from 100 % to 195.35 % for Cyt-*c*, respectively. It indicated the enhanced bio-electricity generation ability of *MJ2* during the domestication process (Heidary et al., 2020).

To further quantify the two electron mediators detected in the electrochemical characterization, the flavins and Cyt-*c* production were determined, and the result was shown in Fig. 3H. There was no significant difference in flavins production as the cycle index increased ($P > 0.05$), and probably due to the formation of a stable biofilm structure during the domestication of *MJ2*, which is mainly dependent on the biofilm for the EET, and the smaller role of flavin in the EET process (Yang et al., 2022b). In contrast, the production of Cyt-*c* increased significantly with the index of cycles ($P < 0.05$). As mentioned previously, it has been reported that EET via biofilm was mediated by Cyt-*c* in the OM, so the increased Cyt-*c* production also facilitated the formation of the stable biofilm.

3.4. Comparative genomic analysis of MJ2

3.4.1. Characteristics of complete genome of MJ2

To clarify the whole electron transfer pathway of *MJ2*, the complete genome sequence of *MJ2* was analyzed to obtain more insights into the substance and energy metabolism information. The genomic features of *MJ2* were showed in Table 2, the final assembly of *MJ2* genome showed that the complete genome size of 2.99 Mbp with G + C content of 33.73 %, and genome annotation yielded 3106 coding genes, 15 rRNA genes, 57 tRNA genes and 5 sRNA genes. In addition, 17 genomic islands and 5 prophages were matched. Based on the above genome components, the genome structure circle of *MJ2* was mapped.

Besides, the coding genes spliced in the above sequencing process were functional annotations using Clusters of Orthologous Groups (COG), Kyoto Encyclopedia of Genes and Genomes (KEGG), Gene Ontology (GO), Non-Redundant Protein Database (NR), Swiss-Prot, Pfam, Transporter Classification Database (TCDB), Carbohydrate-Active enZYmes Database (CAZy), and the result was shown in Table S1. The substance and energy metabolize pathways of *MJ2* were constructed using known metabolic pathways in above database to map its IET pathways. Based on the genomic information of *MJ2*, it was shown that a conventional CoQ-containing electron transfer chain involving flavins and Cyt-*c* was present in the IET of *MJ2* (Fig. S5).

3.4.2. Effect of electron mediators on electron transfer of MJ2

To investigate whether the EET of *MJ2* passed through the above conventional electron transfer chain, the corresponding specific respiratory inhibitors were added to the anode solution of MFC to determine its effect on electron transfer of *MJ2*. The addition of capsaicin, rotenone and dicumarol had no significant effect on ETSA ($P > 0.05$), and these phenomena suggest that the transfer of electrons from intracellular to extracellular in *MJ2* may not be via this electron transfer chain. However, the addition of famoxadone significantly inhibited ETSA (Fig. 4A), suggesting that inhibition of electron transfer to Cyt-*c* could significantly reduce ETSA. It has been reported that some hydrogen-producing *Clostridium* with the EET ability (Xiao et al., 2018). In order to verify the existence of hydrogenase pathway in *MJ2*, the H* quencher TBA was added to determine its effect on ETSA, and as we expected, the addition of TBA also significantly reduced ETSA. In addition, the simultaneous addition of famoxadone and TBA further reduced ETSA, indicating that the two inhibitors have a synergistic effect on this electron transfer chain. In contrast, the addition of flavins did not significantly affect ETSA, which is consistent with the results of bio-electricity generation, indicating that flavins are not a key factor in the bio-electricity generation of *MJ2*. However, ETSA could be significantly increased after the addition of Cyt-*c*, suggesting that Cyt-*c* is involved in the IET process of *MJ2*.

The hydrogenase activity was further measured, and the result was shown in Fig. 4B. Both TBA and famoxadone were able to inhibit hydrogenase activity, and their inhibition of hydrogenase activity had a synergistic effect, while the addition of Cyt-*c* was able to significantly promote hydrogenase activity (104.92 mL-H_2/g-cell protein), suggesting that Cyt-*c* is related to hydrogenase activity. It is inferred that the hydrogenase in *MJ2* contains Cyt-*c* hydrogenase (EC 1.12.2.1), which uses Cyt-*c* as a coenzyme and is present in IM or PS of sulfate-reducing bacteria (Yang et al., 2020).

Meanwhile, the effects of various inhibitors on the bio-electricity generation performance were shown in Fig. 4C. The effects of adding capsaicin, rotenone and dicumarol on the bio-electricity generation performance were not significant, while the addition of famoxadone and TBA had inhibitory effects on it, indicating that they also had inhibitory effects on the EET performance. It can be seen that the addition of famoxadone, TBA or their combinations was able to reduce the peak voltage and output voltage difference (Table S2). The peak voltage was only 91.41 mV for both additions, while the addition of Cyt-*c* significantly promoted the bio-electricity generation, increasing the peak voltage to 307.55 mV. Furthermore, the addition of flavins had no significant effect on the bio-electricity generation properties, which also indicated that flavins were not involved in EET, while Cyt-*c* played an important role in EET. Cyt-*c* uses heme c containing iron porphyrins as a cofactor and is a soluble cytochrome, which can act as an electron shuttle mediator or terminal reductase (Lowe et al., 2010; Myers and Myers, 1992).

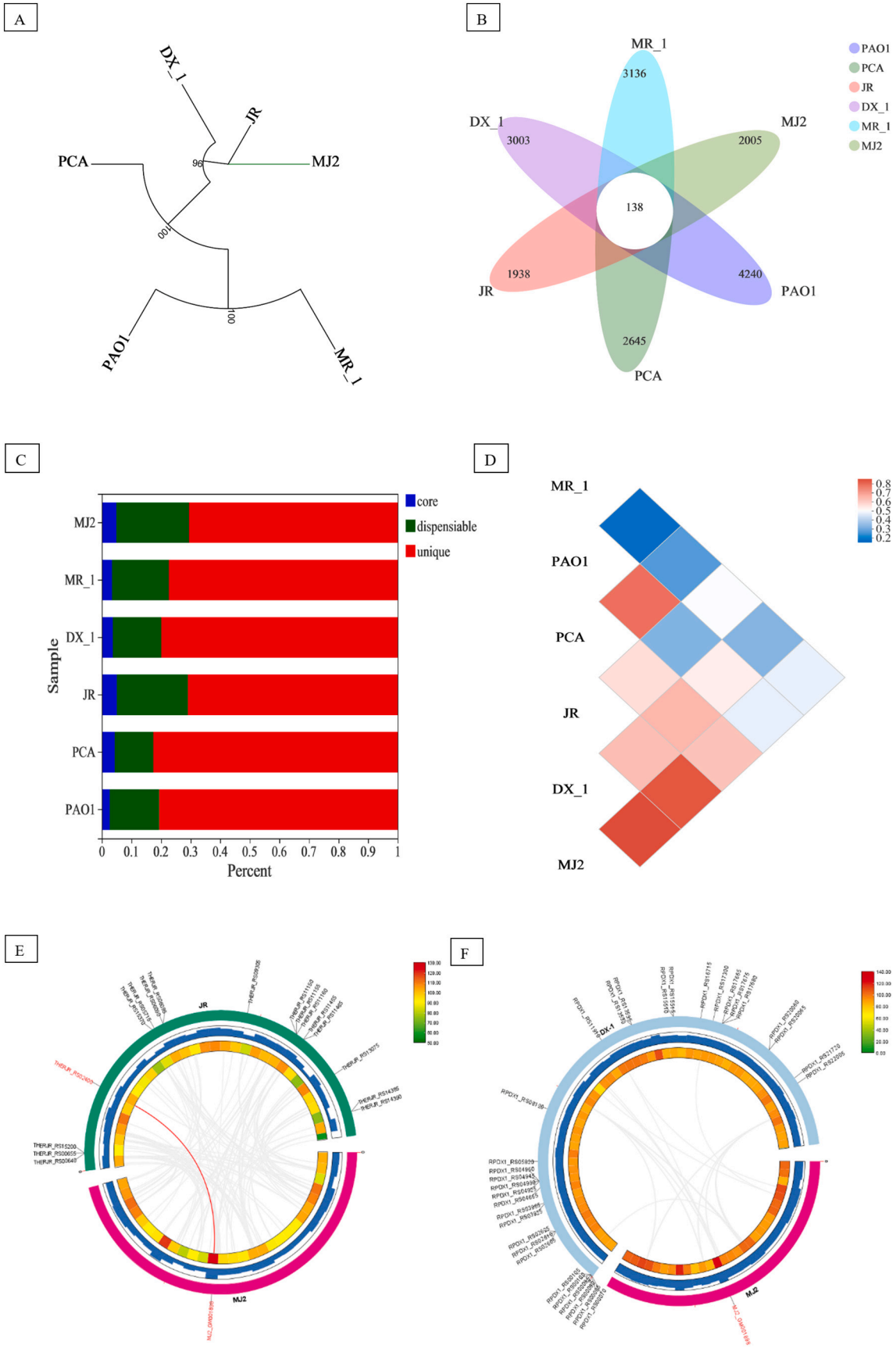

Fig. 5. Comparative genomic analysis between *MJ2* and other typical exoelectrogens. (A) Phylogenetic tree; (B) Veen diagram of core and unique clusters; (C) Pan-genomic cluster distribution; (D) ANI-based matrix heatmap; (E) Genomic synteny between *MJ2* and *JR*; (F) Genomic synteny between *MJ2* and *DX-1*.

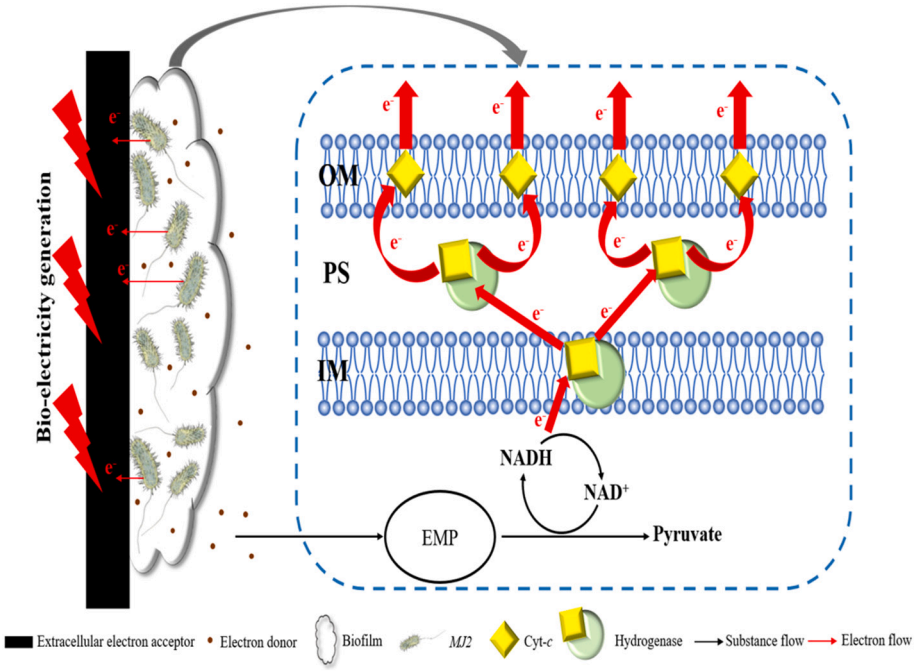

Fig. 6. Proposed schematic of the EET mechanism of *MJ2*.

3.4.3. *Cyt-c gene specificity of MJ2*

To elucidate the function of Cyt-*c* in the electron transfer of *MJ2*, comparative genomic analysis was performed on several typical exoelectrogens, which transferred electrons to extracellular by the biofilm and used Cyt-*c* as an electron shuttle mediator. The complete genome sequence of six exoelectrogens was analyzed to obtain more insight into the genetic information, and the result was shown in Table 2. Besides, the evolutionary status of the six strains was analyzed, and a phylogenetic tree was constructed with 16 S rDNA as shown in Fig. 5A, from which it is clear that *MJ2* has a closer phylogenetic relationship with *JR* and a more distant affinity with *PAO1* and *MR-1*, which may be due to the fact that *MJ2* belongs to the same *Firmicutes* as *JR*, while *PAO1* and *MR-1* belong to the same *Proteobacteria*, and the bacterial taxonomy represents its distant affinities (Torres et al., 2009). In addition, a pan-genome analysis of these six microorganisms showed that there were only 138 core genes in these six strains (Fig. 5B), and the percentage of unique genes was high in the whole genome, indicating that although all of these six strains had electrical production properties, the uniqueness of their respective genomes was high. Among these six strains, *MJ2* had the least number of non-redundant specific genes with *JR*. The core genes can reflect the similarity of microbial phenotypes (Fig. 5C). ANI analysis of core genes showed that *MJ2* had the highest similarity with *DX-1*, and *MJ2* had the second highest similarity with *JR*, indicating that the bio-electricity generation activity of *MJ2* is functionally similar to *JR* or *DX-1* (Fig. 5D). Establishing the linkage of genomic synteny between *MJ2* and *DX-1* and *JR* (Fig. 5E–F), respectively, showed that there are more synteny regions between the genomes of *MJ2* and *JR*, and these regions may be associated with some of their phenotypes. In contrast, there were fewer regions of synteny between *MJ2* and *DX-1* (gray linkage), indicating that the two have fewer similar phenotypes. The regions associated with Cyt-*c* function were identified in the genome sequences of the three microorganisms separately and annotated on the genome. Further analysis of Cyt-*c* gene was performed, and a fragment with synteny with Cyt-*c* gene (red linkage) was found on the genome of *JR*, while this region was not found in *DX-1*, indicating that Cyt-*c* in *MJ2* is functionally similar to Cyt-*c* in *JR*, while in *JR*, THERJR-RS02400, which controls Cyt-*c* synthesis (Table S3), shuttles between the inner and outer membrane to mediate electron transfer, and is able to bind to the outer membrane to mediate electrons transfer (Byrne-Bailey et al., 2010). However, there is only one gene controlling Cyt-*c* synthesis in *MJ2*, unlike other exoelectrogens with multihaem Cyt-*c*. This results in fewer electron transfer pathways, but the IET in *MJ2* is via NADH to the hydrogenase of the IM or PS, and the Cyt-*c* on the hydrogenase can shuttle from the IM to the OM, mediating the formation of biofilm. Therefore, it could directly get the electron from hydrogenase, instead of the CoQ-involved long electron transfer chain. In this way, the electron transfer distance was greatly shortened, leading to a significant improvement in electron transfer efficiency.

3.5. *Proposed mechanism of electron transfer in MJ2 and the significance of this study*

The mechanism of electron transfer in *MJ2* was shown in Fig. 6. Here, the IET pathway of *MJ2* does not pass through the conventional respiratory chain, but through the hydrogenase with Cyt-*c* as the coenzyme, which transfers electrons from NADH generated by intracellular oxidized electron donor to Cyt-*c*. Intracellular electrons obtained from Cyt-*c* on the IM were shuttled through the PS to Cyt-*c* bound to the OM. Since *MJ2* formed a biofilm on the electrode surface, it leads to direct contact with the extracellular electron acceptor, thus transferring electrons from Cyt-*c* widely distributed on the OM directly to the extracellular electron acceptor. This shortens the distance of electron transfer and improves the efficiency of electron transfer to the extracellular. The mechanism of electron transfer proposed in this study provides new insight into exploring the diversity of extracellular respiration.

4. Conclusion

This study demonstrated that *T. thermosaccharolyticum MJ2* showed extracellular Fe(III) and electrode respiration ability. Notably, a novel electron transfer pathway via Cyt-*c*/hydrogenase-based was proposed in *T. thermosaccharolyticum MJ2*, which effectively shortens the EET route. Meanwhile, the exogenous Cyt-*c* increased hydrogenase activity and bio-electricity generation performance. Moreover, the Cyt-*c* of the outer membrane mediates the formation of biofilms for the direct transfer of electrons to the extracellular electron acceptor. However, the role of

Cyt-*c* was only roughly investigated. Mostly, the function of extracted and purified Cyt-*c* needed further exploration.

CRediT authorship contribution statement

Xing Yan: Conceptualization, Methodology, Software, Validation, Formal analysis, Investigation, Data curation, Writing - original draft.

Jie Bu: Resources, Writing - review & editing.

Xiong Chen: Resources, Writing - review & editing.

Ming-Jun Zhu: Resources, Writing - review & editing, Supervision, Project administration, Funding acquisition.

Declaration of competing interest

The authors declare that they have no known competing financial interests or personal relationships that could have appeared to influence the work reported in this paper.

Data availability

Data will be made available on request.

Acknowledgements

The authors gratefully acknowledge the financial support of the National Natural Science Foundation of China [grant no. 52070079], and Open Project Funding of the Key Laboratory of Fermentation Engineering (Ministry of Education) [grant no. 202105FE01].

Appendix A. Supplementary data

Supplementary data to this article can be found online at https://doi.org/10.1016/j.scitotenv.2023.167294.

References

An, Q., Wang, J.L., Wang, Y.T., Lin, Z.L., Zhu, M.J., 2018. Investigation on hydrogen production from paper sludge without inoculation and its enhancement by Clostridium thermocellum. Bioresour. Technol. 263, 120–127. https://doi.org/10.1016/j.biortech.2018.04.105.

Anderson, R.T., Vrionis, H.A., Ortiz-Bernad, I., Resch, C.T., Long, P.E., Dayvault, R., et al., 2003. Stimulating the in situ activity of Geobacter species to remove uranium from the groundwater of a uranium-contaminated aquifer. Appl. Environ. Microbiol. 69, 5884–5891. https://doi.org/10.1128/AEM.69.10.5884-5891.2003.

Bu, J., Wei, H.L., Wang, Y.T., Cheng, J.R., Zhu, M.J., 2021. Biochar boosts dark fermentative H2 production from sugarcane bagasse by selective enrichment/colonization of functional bacteria and enhancing extracellular electron transfer. Water Res. 202, 117440. https://doi.org/10.1016/j.watres.2021.117440.

Bu, J., Hu, B.B., Wu, H.Z., Zhu, M.J., 2022. Improved methane production with redox-active/conductive biochar amendment by establishing spatial ecological niche and mediating electron transfer. Bioresour. Technol. 351, 127072. https://doi.org/10.1016/j.biortech.2022.127072.

Byrne-Bailey, K.G., Wrighton, K.C., Melnyk, R.A., Agbo, P., Hazen, T.C., Coates, J.D., 2010. Complete genome sequence of the electricity-producing "Thermincola potens" strain JR. J. Bacteriol. 192, 4078–4079. https://doi.org/10.1128/JB.00044-10.

Chen, C., Chen, H., Zhang, Y., Thomas, H.R., Frank, M.H., He, Y., et al., 2020. TBtools: an integrative toolkit developed for interactive analyses of big biological data. Mol. Plant 13, 1194–1202. https://doi.org/10.1016/j.molp.2020.06.009.

Coursolle, D., Baron, D.B., Bond, D.R., Gralnick, J.A., 2010. The Mtr respiratory pathway is essential for reducing flavins and electrodes in Shewanella oneidensis. J. Bacteriol. 192, 467–474. https://doi.org/10.1128/JB.00925-09.

Dai, K., Wen, J.L., Zhang, F., Ma, X.W., Cui, X.Y., Zhang, Q., et al., 2017. Electricity production and microbial characterization of thermophilic microbial fuel cells. Bioresour. Technol. 243, 512–519. https://doi.org/10.1016/j.biortech.2017.06.167.

Davila, D., Esquivel, J.P., Sabate, N., Mas, J., 2011. Silicon-based microfabricated microbial fuel cell toxicity sensor. Biosens. Bioelectron. 26, 2426–2430. https://doi.org/10.1016/j.bios.2010.10.025.

Dopson, M., Ni, G., Sleutels, T.H., 2016. Possibilities for extremophilic microorganisms in microbial electrochemical systems. FEMS Microbiol. Rev. 40, 164–181. https://doi.org/10.1093/femsre/fuv044.

Gonzalez-Gil, G., Amonette, J.E., Romine, M.F., Gorby, Y.A., Geesey, G.G., 2005. Bioreduction of natural specular hematite under flow conditions. Geochim. Cosmochim. Acta 69, 1145–1155. https://doi.org/10.1016/j.gca.2004.08.014.

Hallbeck, L., Pedersen, K., 1990. Culture parameters regulating stalk formation and growth rate of Gallionella ferruginea. J. Gen. Microbiol. 136, 1675–1680. https://doi.org/10.1099/00221287-136-9-1675.

Hassan, H., Jin, B., Donner, E., Vasileiadis, S., Saint, C., Dai, S., 2018. Microbial community and bioelectrochemical activities in MFC for degrading phenol and producing electricity: microbial consortia could make differences. Chem. Eng. J. 332, 647–657. https://doi.org/10.1016/j.cej.2017.09.114.

Heidary, N., Kornienko, N., Kalathil, S., Fang, X., Ly, K.H., Greer, H.F., et al., 2020. Disparity of cytochrome utilization in anodic and cathodic extracellular electron transfer pathways of geobacter sulfurreducens biofilms. J. Am. Chem. Soc. 142, 5194–5203. https://doi.org/10.1021/jacs.9b13077.

Hols, P., Hancy, F., Fontaine, L., Grossiord, B., Prozzi, D., Leblond-Bourget, N., et al., 2005. New insights in the molecular biology and physiology of Streptococcus thermophilus revealed by comparative genomics. FEMS Microbiol. Rev. 29, 435–463. https://doi.org/10.1016/j.femsre.2005.04.008.

Huang, J., Zhu, N., Cao, Y., Peng, Y., Wu, P., Dong, W., 2015. Exoelectrogenic bacterium phylogenetically related to Citrobacter freundii, isolated from anodic biofilm of a microbial fuel cell. Appl. Biochem. Biotechnol. 175, 1879–1891. https://doi.org/10.1007/s12010-014-1418-9.

Huang, J.R., Chen, X., Hu, B.B., Cheng, J.R., Zhu, M.J., 2022. Bioaugmentation combined with biochar to enhance thermophilic hydrogen production from sugarcane bagasse. Bioresour. Technol. 348, 126790. https://doi.org/10.1016/j.biortech.2022.126790.

Jia, Y., Qian, D., Chen, Y., Hu, Y., 2021. Intra/extracellular electron transfer for aerobic denitrification mediated by in-situ biosynthesis palladium nanoparticles. Water Res. 189, 116612. https://doi.org/10.1016/j.watres.2020.116612.

Koch, C., Harnisch, F., 2016. Is there a specific ecological niche for electroactive microorganisms? Chem Electro Chem 3, 1282–1295. https://doi.org/10.1002/celc.201600079.

Koffi, N.D.J., Okabe, S., 2020. Domestic wastewater treatment and energy harvesting by serpentine up-flow MFCs equipped with PVDF-based activated carbon air-cathodes and a low voltage booster. Chem. Eng. J. 380, 122443. https://doi.org/10.1016/j.cej.2019.122443.

Kondo, K., Okamoto, A., Hashimoto, K., Nakamura, R., 2015. Sulfur-mediated electron shuttling sustains microbial long-distance extracellular electron transfer with the aid of metallic iron sulfides. Langmuir 31, 7427–7434. https://doi.org/10.1021/acs.langmuir.5b01033.

Kugarajah, V., Dharmalingam, S., 2021. Effect of silver incorporated sulphonated poly ether ether ketone membranes on microbial fuel cell performance and microbial community analysis. Chem. Eng. J. 415, 128961. https://doi.org/10.1016/j.cej.2021.128961.

Lee, L.Y., Ong, S.L., Ng, W.J., 2004. Biofilm morphology and nitrification activities: recovery of nitrifying biofilm particles covered with heterotrophic outgrowth. Bioresour. Technol. 95, 209–214. https://doi.org/10.1016/j.biortech.2003.05.004.

Li, H., Wang, B., Deng, S., Dai, J., Shao, S., 2019a. Oxygen-containing functional groups on bioelectrode surface enhance expression of c-type cytochromes in biofilm and boost extracellular electron transfer. Bioresour. Technol. 292, 121995. https://doi.org/10.1016/j.biortech.2019.121995.

Li, Z., Liu, B., Cui, H., Ding, J., Li, H., Xie, G., et al., 2019b. The complete genome sequence of Ethanoligenens harbinense reveals the metabolic pathway of acetate-ethanol fermentation: a novel understanding of the principles of anaerobic biotechnology. Environ. Int. 131, 105053. https://doi.org/10.1016/j.envint.2019.105053.

Lian, J., Tian, X., Guo, J., Guo, Y., Song, Y., Yue, L., et al., 2016. Effects of resazurin on perchlorate reduction and bioelectricity generation in microbial fuel cells and its catalysing mechanism. Biochem. Eng. J. 114, 164–172. https://doi.org/10.1016/j.bej.2016.06.028.

Liu, X., Jing, X., Ye, Y., Zhan, J., Ye, J., Zhou, S., 2019. Bacterial vesicles mediate extracellular electron transfer. Environ. Sci. Technol. Lett. 7, 27–34. https://doi.org/10.1021/acs.estlett.9b00707.

Logan, B.E., Rossi, R., Ragab, A., Saikaly, P.E., 2019. Electroactive microorganisms in bioelectrochemical systems. Nat. Rev. Microbiol. 17, 307–319. https://doi.org/10.1038/s41579-019-0173-x.

Lovley, D.R., Phillips, E.J., 1988. Novel mode of microbial energy metabolism: organic carbon oxidation coupled to dissimilatory reduction of iron or manganese. Appl. Environ. Microbiol. 54, 1472–1480. https://doi.org/10.1128/aem.54.6.1472-1480.1988.

Lovley, D.R., Holmes, D.E., Nevin, K.P., 2004. Dissimilatory Fe(III) and Mn(IV) reduction. Adv. Microb. Physiol. 49, 219–286. https://doi.org/10.1016/S0065-2911(04)49005-5.

Lowe, E.C., Bydder, S., Hartshorne, R.S., Tape, H.L., Dridge, E.J., Debieux, C.M., et al., 2010. Quinol-cytochrome c oxidoreductase and cytochrome c4 mediate electron transfer during selenate respiration in Thauera selenatis. J. Biol. Chem. 285, 18433–18442. https://doi.org/10.1074/jbc.M110.115873.

Lu, H., Zhou, Y., Fu, Z., Wang, X., Zhou, J., Guo, W., 2022. Mutual interaction between the secreted flavins and immobilized quinone in anaerobic removal of high-polarity aromatic compounds containing nitrogen by Shewanella sp. RQs-106. J. Hazard. Mater. 431, 128595. https://doi.org/10.1016/j.jhazmat.2022.128595.

Lusk, B.G., Khan, Q.F., Parameswaran, P., Hameed, A., Ali, N., Rittmann, B.E., et al., 2015. Characterization of electrical current-generation capabilities from thermophilic bacterium Thermoanaerobacter pseudethanolicus using xylose, glucose, cellobiose, or acetate with fixed anode potentials. Environ. Sci. Technol. 49, 14725–14731. https://doi.org/10.1021/acs.est.5b04036.

Lusk, B.G., Colin, A., Parameswaran, P., Rittmann, B.E., Torres, C.I., 2018. Simultaneous fermentation of cellulose and current production with an enriched mixed culture of thermophilic bacteria in a microbial electrolysis cell. J. Microbial. Biotechnol. 11, 63–73. https://doi.org/10.1111/1751-7915.12733.

Michie, I.S., Kim, J.R., Dinsdale, R.M., Guwy, A.J., Premier, G.C., 2011. Operational temperature regulates anodic biofilm growth and the development of electrogenic activity. Appl. Microbiol. Biotechnol. 92, 419–430. https://doi.org/10.1007/s00253-011-3531-9.

Myers, C.R., Myers, J.M., 1992. Localization of cytochromes to the outer membrane of anaerobically grown Shewanella putrefaciens MR-1. J. Bacteriol. 174, 3429–3438. https://doi.org/10.1128/jb.174.11.3429-3438.1992.

Myers, C.R., Nealson, K.H., 1988. Microbial reduction of manganese oxides: interactions with iron and sulfur. Geochim. Cosmochim. Acta 52, 2727–2732. https://doi.org/10.1016/0016-7037(88)90041-5.

Parameswaran, P., Bry, T., Popat, S.C., Lusk, B.G., Rittmann, B.E., Torres, C.I., 2013. Kinetic, electrochemical, and microscopic characterization of the thermophilic, anode-respiring bacterium Thermincola ferriacetica. Environ. Sci. Technol. 47, 4934–4940. https://doi.org/10.1021/es400321c.

Saunders, S.H., Tse, E.C.M., Yates, M.D., Otero, F.J., Trammell, S.A., Stemp, E.D.A., et al., 2020. Extracellular DNA promotes efficient extracellular electron transfer by pyocyanin in Pseudomonas aeruginosa biofilms. Cell 182, 919–932 e19. https://doi.org/10.1016/j.cell.2020.07.006.

Shen, X., Ma, R., Huang, Y., Chen, L., Xu, Z., Li, D., et al., 2020. Nano-decocted ferrous polysulfide coordinates ferroptosis-like death in bacteria for anti-infection therapy. Nano Today 35, 100981. https://doi.org/10.1016/j.nantod.2020.100981.

Stookey, L.L., 1970. Ferrozine—a new spectrophotometric reagent for iron. Anal. Chem. 42, 779–781. https://doi.org/10.1021/ac60289a016.

Torres, C.I., Krajmalnik-Brown, R., Parameswaran, P., Marcus, A.K., Wanger, G., Gorby, Y.A., et al., 2009. Selecting anode-respiring bacteria based on anode potential: phylogenetic, electrochemical, and microscopic characterization. Environ. Sci. Technol. 43, 9519–9524. https://doi.org/10.1021/es902165y.

Wang, X., Roger, M., Clement, R., Lecomte, S., Biaso, F., Abriata, L.A., et al., 2018. Electron transfer in an acidophilic bacterium: interaction between a diheme cytochrome and a cupredoxin. Chem. Sci. 9, 4879–4891. https://doi.org/10.1039/c8sc01615a.

Wang, J., Lin, W., Chen, Y., Hu, Y., Luo, Q., 2021. Prompting the FDH/Hases-based electron transfers during Pt(IV) reduction mediated by bio-Pd(0). J. Hazard. Mater. 417, 126090. https://doi.org/10.1016/j.jhazmat.2021.126090.

Weber, K.A., Achenbach, L.A., Coates, J.D., 2006. Microorganisms pumping iron: anaerobic microbial iron oxidation and reduction. Nat. Rev. Microbiol. 4, 752–764. https://doi.org/10.1038/nrmicro1490.

Wu, X., Qiao, Y., Shi, Z., Tang, W., Li, C.M., 2018. Hierarchically porous N-doped carbon nanotubes/reduced graphene oxide composite for promoting flavin-based interfacial electron transfer in microbial fuel cells. ACS Appl. Mater. Interfaces 10, 11671–11677. https://doi.org/10.1021/acsami.7b19826.

Xiao, L., Liu, F., Liu, J., Li, J., Zhang, Y., Yu, J., et al., 2018. Nano-Fe3O4particles accelerating electromethanogenesis on an hour-long timescale in wetland soil. Environ. Sci. Nano 5, 436–445. https://doi.org/10.1039/c7en00577f.

Yang, Z.N., Hou, Y.N., Zhang, B., Cheng, H.Y., Yong, Y.C., Liu, W.Z., et al., 2020. Insights into palladium nanoparticles produced by Shewanella oneidensis MR-1: roles of NADH dehydrogenases and hydrogenases. Environ. Res. 191, 110196. https://doi.org/10.1016/j.envres.2020.110196.

Yang, K., Wang, X., Yi, Y., Ma, J., Ning, P., 2022a. Formulation of NZVI-supported lactic acid/PAN membrane with glutathione for enhanced dynamic Cr(VI) removal. J. Clean. Prod. 363, 132350. https://doi.org/10.1016/j.jclepro.2022.132350.

Yang, Y., Fang, A., Feng, K., Zhang, D., Zhou, H., Xing, D., 2022b. Single-cell metagenomics and metagenomics approaches reveal extracellular electron transfer of psychrophilic electroactive biofilms. Sci. Total Environ. 836, 155606. https://doi.org/10.1016/j.scitotenv.2022.155606.

Yates, M.D., Kiely, P.D., Call, D.F., Rismani-Yazdi, H., Bibby, K., Peccia, J., et al., 2012. Convergent development of anodic bacterial communities in microbial fuel cells. ISME J. 6, 2002–2013. https://doi.org/10.1038/ismej.2012.42.

Yin, Q., Yang, S., Wang, Z., Xing, L., Wu, G., 2018. Clarifying electron transfer and metagenomic analysis of microbial community in the methane production process with the addition of ferroferric oxide. Chem. Eng. J. 333, 216–225. https://doi.org/10.1016/j.cej.2017.09.160.

Zhuang, Z., Yang, G., Mai, Q., Guo, J., Liu, X., Zhuang, L., 2020. Physiological potential of extracellular polysaccharide in promoting Geobacter biofilm formation and extracellular electron transfer. Sci. Total Environ. 741, 140365. https://doi.org/10.1016/j.scitotenv.2020.140365.